



New quercetin-coated titanate nanotubes and their radiosensitization effect on human bladder cancer

Luisa Alban^a, Wesley Formentin Monteiro^a, Fernando Mendonça Diz^a, Gabriela Messias Miranda^a, Carolina Majolo Scheid^a, Eduardo Rosa Zotti^b, Fernanda Bueno Morrone^c, Rosane Ligabue^{a,d,*}

^a Graduate Program in Materials Engineering and Technology, Pontifical Catholic University of Rio Grande do Sul - PUCRS, Brazil

^b School of Technology, Pontifical Catholic University of Rio Grande do Sul - PUCRS, Brazil

^c School of Health Sciences, Pontifical Catholic University of Rio Grande do Sul - PUCRS, Brazil

^d School of Sciences, Pontifical Catholic University of Rio Grande do Sul - PUCRS, Brazil

ARTICLE INFO

Keywords:

Titanate nanotubes
Quercetin
Radiosensitization
Bladder cancer

ABSTRACT

Interest in nanostructures such as titanate nanotubes (TNT) has grown notably in recent years due to their biocompatibility and economic viability, making them promising for application in the biomedical field. Quercetin (Qc) has shown great potential as a chemopreventive agent and has been widely studied for the treatment of diseases such as bladder cancer. Motivated by the possibilities of developing a new hybrid nanostructure with potential in biomedical applications, this study aimed to investigate the incorporation of quercetin in sodium (NaTNT) and zinc (ZnTNT) titanate nanotubes, and characterize the nanostructures formed. Qc release testing was also performed and cytotoxicity in Vero and T24 cell lines evaluated by the MTT assay. The effect of TNTs on T24 bladder cancer cell radiosensitivity was also assessed, using cell proliferation and a clonogenic assay. The TNT nanostructures were synthesized and characterized by FESEM, EDS, TEM, FTIR, XRD and TGA. The results showed that the nanostructures have a tubular structure and that the exchange of Na⁺ ions for Zn²⁺ and incorporation of quercetin did not alter this morphology. In addition, interaction between Zn and Qc increased the thermal stability of the nanostructures. The release test showed that maximum Qc delivery occurred after 24 h and the presence of Zn controlled its release. Biological assays indicated that the NaTNTQc and ZnTNTQc nanostructures decreased the viability of T24 cells after 48 h at high concentrations. Furthermore, the clonogenic assay showed that NaTNT, NaTNTQc, ZnTNT and ZnTNTQc combined with 5 Gy reduced the formation of polyclonal colonies of T24 cells after 48 h. The results suggest that the nanostructures synthesized in this study interfere in cell proliferation and can therefore be a powerful tool in the treatment of bladder cancer.

1. Introduction

Bladder cancer (BC) is the second most common urinary tract malignancy in the world, with the ninth highest incidence, at 430,000 new cases annually [1,2]. It can be categorized as non-muscle-invasive (NMIBC) or muscle-invasive (MIBC) in 75 and 25% of cases, respectively [3,4]. MIBC or metastatic disease is the clinical stage most lethal [5,6].

For decades, radical cystectomy with bilateral pelvic lymphadenectomy has been the gold standard surgical treatment for MIBC [7,8], but has high rates of morbidity and postoperative complications [8,9]. Trimodal therapy is an alternative approach that demonstrated a median 5-year survival of 57% of patients submitted to multimodal

therapy versus 52% undergoing radical cystectomy [10]. Trimodal treatment is a combination of surgery (transurethral bladder tumor resection), chemotherapy and radiotherapy [9,11,12]. With respect to the non-surgical parameters of this therapy, tumor response to chemoradiation therapy is superior to that of radiation therapy alone [9]. In this respect, it is important to gain a better understanding of the disease process and explore new tools to improve radiotherapy efficacy.

The search for strategies capable of eliminating cancer cells is one of the greatest medical challenges and as such, nanotechnology has been the focus of increasing attention [13]. Nanomedicine is an emerging area of nanotechnology applied to disease diagnosis, treatment and monitoring, and the unique properties make nanotechnology an important medical revolution [14–19]. Nanomaterials are effective

* Corresponding author at: Graduate Program in Materials Engineering and Technology, Pontifical Catholic University of Rio Grande do Sul - PUCRS, Brazil.
E-mail address: rligabue@pucrs.br (R. Ligabue).

carriers of multiple therapeutic and diagnostic agents and the various types, including nanoparticles, quantum dots and superparamagnetic nanoparticles, are used in cancer treatment [20–22].

A range of nanomaterials has been studied and important results have been obtained with hybrid nanomaterials such as metal-based hybrid nanoparticles (MHNs). High-Z elements and functional components such as noble metals and organic materials not only enhance radiation, but also act as important biomedical agents [23]. Some examples reported in the literature include core-shell gold and selenium applied to radiation therapy [24] and quantum dots or nanocrystals to photothermal therapy [25,26].

On the other hand, quercetin is a natural flavonoid that can be extracted from apples, wine and tea. Medical applications include the treatment of soft tissue injuries and cancer cell growth inhibition [27–29]. Moreover, some studies have shown that treating cancer cells with quercetin leads to apoptotic effects by activating the mitochondrial pathway, thereby improving the efficacy of anti-cancer drugs [30–32]. The use of quercetin carrier systems is just one of the innovative possibilities provided by nanomedicine. Silica-based hybrid systems with quercetin have shown promising results in neurodegeneration [33]. Hybrid systems using different silica supports (SBA15, SBA 16 and MCM-41) and quercetin in dermal formulations have also been studied [34,35]. Research on the use of quercetin as a functional component poses new challenges, characterized by the development of systems that can be used as support for future investigations.

Titanate nanotubes (TNTs) are hollow multiwall nanostructures with a unique morphology and easily modifiable structure [36,37], making them useful in several fields, as catalysts [38–40], fillers in polymer matrices [41,42], and antibacterial nanomaterial [43], among others. In addition, studies on TNT application in nanomedicine have demonstrated their biocompatibility and cytotoxicity to tumor cells, in addition to enhancing the efficacy of radiation therapy [44–47]. However, to date there are no studies that describe titanate nanotubes as nanocarrier of quercetin in nanomedicine. In this context, and in order to contribute to nanomedicine research for cancer treatment, the present study aims to synthesize new hybrid nanostructures with quercetin-coated titanate nanotubes (NaTNTQc and ZnTNTQc) and evaluate their action in invasive muscle bladder cancer cells (T24) associated with radiotherapy.

2. Methods

2.1. Materials

Titanium dioxide (JB Química, TiO₂, 98% anatase phase), sodium hydroxide (Vetec, 99%), zinc chloride (Vetec, 99%), dimethyl sulfoxide, DMSO (Sigma-Aldrich, 99,5%) and quercetin (Sigma-Aldrich, 95%) were used as received. The following materials were used for cellular management: RPMI and DMEM media (Dulbecco's Modified Eagle Medium), fetal bovine serum (FBS), penicillin-streptomycin (10,000 U/mL), and amphotericin B (Fungizone), obtained from Gibco, MTT (3-(4,5-dimethylthiazol-2-yl)-2,5-diphenyltetrazolium bromide solution – MTT 5 mg/mL in PBS and 90% culture medium supplemented with 10% FBS), and calcium and magnesium-free medium (CMF).

2.2. Preparation of nanostructures

Sodium titanate nanotubes (NaTNT) were synthesized using the hydrothermal method, as described in the literature [48,49]. In a typical procedure, 1.5 g (18.7 mmol) of TiO₂ was added to 120 mL of 10 mol.L⁻¹ NaOH aqueous solution under magnetic stirring, for 30 min at room temperature. The solution was then transferred to a stainless steel reactor (200 cm³) internally coated in Teflon®, and maintained at 135 °C for 72 h. Next, a white precipitate was separated by centrifugation, washed with distilled water until pH = 8, dried at 80 °C for 6 h and placed in a desiccator. Titanate nanotubes synthesis with zinc

(ZnTNT) was based on the method described in the literature [34]. A typical procedure consisted of adding 0.5 g (1.65 mmol) of NaTNT to 100 mL of a 0.5 mol.L⁻¹ ZnCl₂ aqueous solution (50 mmol) under magnetic stirring, for 15 min at room temperature. Next, the suspension was filtered under reduced pressure and washed with distilled water until complete chloride ion removal (silver nitrate test). The white solid obtained was dried at 80 °C for 12 h and placed in a desiccator.

The preparation of quercetin-coated titanate nanotubes (NaTNTQc and ZnTNTQc) was adapted from a method described in the literature [34]. To prepare NaTNTQc, 0.5 g (1.66 mmol) of NaTNT and 0.5 g (1.65 mmol) of quercetin were added to 50 mL of ethanol under magnetic stirring, for 60 min at room temperature. The suspension was then centrifuged and the orange solid obtained washed 3 times with 25 mL of distilled water. Next, the solid was dried at 40 °C for 12 h and stored in a desiccator. ZnTNTQc (brown solid) was obtained from ZnTNT using the same procedure described for NaTNTQc.

2.3. Characterization of nanostructures

The morphology of the quercetin-coated titanate nanotubes was assessed by field emission scanning electron microscopy (FESEM), using samples coated with a thin platinum film via ion sputtering (FESEM, FEI Inspect F50, in the secondary electron beam), and transmission electron microscopy of samples deposited onto 300 mesh carbon film-coated copper grids (TEM, FEI Tecnai G2 T20). Energy dispersive spectroscopy (EDS) was used to qualitatively identify the metals in the nanotubes. The external diameters of nanostructures were obtained by transmission electron microscopy (TEM), using *Image J* software (15 measurements). All samples were analyzed in powder form. Fourier-transform infrared spectroscopy (FTIR) was performed on a PerkinElmer spectrometer (Spectrum One), using powder samples at room temperature in UATR mode, with a range of 4000–650 cm⁻¹. The crystalline structure of titanate nanostructures was analyzed by X-ray diffraction (XRD) (Shimadzu XRD 7000), using copper K α radiation ($\lambda = 1.542 \text{ \AA}$), 40 kV, 30 mA, 5°–70° 2 θ , a scanning speed of 0.02°/min and counting time of 2.0 s. The interlamellar distance was calculated based on Bragg's Law, with a reference peak at $2\theta = 10.5^\circ$ [50]. The thermal stability and quercetin content of TNT nanostructures were evaluated by thermogravimetric analysis (TA Instruments Q600). The percentage of quercetin incorporation was determined by TGA at a heating rate of 10 °C/min, from room temperature to 1000 °C, under nitrogen flow. The samples were analyzed in powder form.

2.4. Drug release tests

Analysis of quercetin release from titanate nanotubes (NaTNTQc and ZnTNTQc) was adapted from methods described in the literature [35,51], whereby 5 mg of TNT-based nanostructures were placed in 50 mL of a PBS/ethanol solution (90:10 v/v; pH = 5.5). The assay was performed at 37 °C and 120 rpm for 7 days, with aliquot collection in the first 12 h of tests, followed by one collection per day. At appropriate time intervals (1, 2, 3, 4, 5, 6, 12, 24 and 48 h), 3 mL samples were taken from the release medium. The medium was replenished with the same volume of fresh PBS/ethanol solution to ensure infinite dilution. The aliquot collected was analyzed using a UV-Vis spectrophotometer (Perkin Elmer Lambda 35, wavelength of 372 nm). The quercetin concentration released was calculated according to a calibration curve, prepared under the same test conditions ($r = 0.9989$).

2.5. Cell lines and cell culture

A human urinary bladder cancer cell line (T24), and normal African green monkey kidney cell (Vero) (American Type Culture Collection) were used for the experiments. The T24 cell lines were maintained in RPMI cell culture medium and Vero cells in DMEM, both supplemented with 10% FBS, 0.5 U/mL of penicillin and streptomycin. The cells were

kept in a humidified cell incubator (37 °C, 5% CO₂, and 95% humidity) until the experiment, when they were lifted from the subconfluent cultures with 0.5% trypsin in 5 mM EDTA, counted on a hemocytometer, and plated at the appropriate density according to the experimental protocol.

2.6. Cell viability by MTT assay

Cell viability was determined by the MTT colorimetric assay for metabolic activity [52,53]. Vero and T24 cell lines were seeded at a density of 5×10^3 cells/well on a 96-well plate, with 100 μ L of culture medium. After 24 h, the cells were treated with different concentrations of Qc, NaTNT, NaTNTQc, ZnTNT and ZnTNTQc (25, 50, 100 and 200 μ g/mL) for 24 and 48 h. Cells treated with medium served solely as controls. At the end of treatment period, the medium was removed, the cells were washed with PBS (pH = 7.2–7.4), added with 100 μ L of MTT and incubated for 3 h. The formazan crystals were dissolved in 100 μ L of DMSO. Optical density was measured in 96-well plates (SpectraMax Plus) at 570 nm. Absorbance was linearly proportional to the number of live cells with active mitochondria. The results were determined as a percentage of the absorbance of treated cells in relation to controls. Four independent experiments were performed for each concentration, all in triplicate. Relative cell viability was expressed as percentage (%) relative to the untreated control cells.

2.7. Evaluation of TNT cell internalization by TEM

T24 cells were seeded in 6-well plates at 100×10^3 cells per well. After 24 h of incubation, the RPMI cell culture media were replaced by 2 mL of fresh medium containing 25 μ g/mL of NaTNT, NaTNTQc, ZnTNT and ZnTNTQc, and incubated for 8 days. Semi-confluent T24 cells were trypsinized, centrifuged and washed twice before adding phosphate buffer (pH 7.2–7.4). Next, the bladder cells were fixed in a mixture of 4% paraformaldehyde and 2.5% glutaraldehyde, buffered with 0.1 M PBS (pH 7.2–7.4) at room temperature, and then postfixed in osmium tetroxide in the same buffer for 45 min before dehydration. Dehydration was performed in a graded acetone series (30–100%) and embedding in araldite (Durcupan ACM, Fluka), for 72 h at 60 °C. Thin sections (100 nm) were stained with 2% uranyl acetate, followed by lead citrate. Ultrastructural analysis was performed by transmission electron microscopy (TEM, FEI Tecnai G2 T20).

2.8. Cytotoxicity of TNT combined with irradiation

The T24 cells (7×10^3 cells/well) were seeded in 24-well plates and grown for 24 h. After confluence, they were treated with 25 μ g/mL NaTNT, NaTNTQc, ZnTNT and ZnTNTQc for 24 and 48 h. After the proposed treatment time for each test group, irradiation was performed with gamma radiation at a single dose of 5 Gy, using a Cobalt source from Theratron Phoenix (Theratronics Ltda., Ontario, Canada), with a distance of 54.5 cm between the source and target. The radiosensitivity of T24 cells was determined by two tests: (a) cell counting, and (b) the clonogenic assay (to determine the effect of radiation after 10 days),

according to the method previously described in the literature [46]. For each treatment condition (control and TNT), a non-irradiated group (0 Gy) corresponded to 100% survival, in order to assess only the cytotoxic effect of ionizing radiation.

After radiation, the T24 cell line was incubated in a cell incubator for 24 h and the biological response assessed based on the number of live cells observed in a cell counter (Countess FL, Life Technologies), using the Trypan Blue dye exclusion protocol [12]. The results were expressed as percentage of live cells in relation to the non-irradiated control group.

A clonogenic assay was performed to evaluate the clinical response. After cell counting, T24 cell lines (2×10^2 cells/well) were plated in 6-well plates with RPMI medium, supplemented with 10% FBS without the respective treatments, and maintained in culture for 10 days. The medium was renovated every 2 days. At the end of the experiment, the cells were washed with PBS, fixed with 4% formaldehyde for 20 min, and stained with gentian violet for 10 min. Next, they were washed twice with PBS and dried at room temperature. The results were expressed as absolute number of colonies. The irradiation dose in this study was determined according to the literature [12,46].

2.9. Statistical analysis

The *in vitro* experiments were repeated at least four times, all in triplicate. Results were expressed as standard error of the mean and assessed for statistical significance by one-way analysis of variance (ANOVA), followed by Tukey's post-hoc test (Prims GraphPAD® 7.0). Significance was set at $p < 0.05$.

3. Results and discussions

Exposure to ionizing radiation does not only affect tumor cells, but also provides a favorable microenvironment for metastatic cells resistant to radiotherapeutic treatment [54–56]. The radiosensitization effect of titanate nanotubes makes them a promising new tool in radiation therapy for cancer treatment [46]. However, further research is needed on the radiosensitization and cytotoxicity mechanisms of TNTs. In the present study, in order to contribute to nanomedical research on bladder cancer treatment, we synthesized titanate nanotubes (NaTNT, and ZnTNT) and quercetin-coated titanate nanotubes (NaTNTQc and ZnTNTQc) to increase the effectiveness of radiotherapy treatment in invasive muscle bladder cancer cells.

The TEM images obtained (Fig. 1) show that titanate nanotubes preserved their tubular morphology after the exchange of sodium ions (Fig. 1a) for zinc (Fig. 1b) and quercetin coating (Fig. 1c, d). Nanotubes modified with zinc (Fig. 1b) have an irregular surface (indicated by arrows in Fig. 1b and c), caused by the presence of zinc. The same is true in ZnTNT nanotubes containing quercetin (Fig. 1d). This effect was also observed after incorporating metals such as Sn, Ce and Pd in titanate nanotubes, attributed to metal-support interaction [57–59]. However, the quercetin-coated NaTNT nanotubes (Fig. 1c) have a similar structure to those without the flavonoid (Fig. 1a), since sodium ions are located primarily in the interlamellar region, unlike zinc ions,

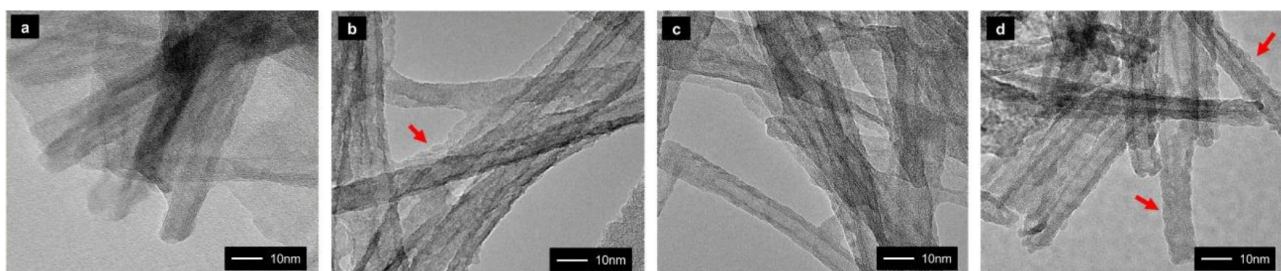


Fig. 1. TEM images for (a) NaTNT, (b) ZnTNT, (c) NaTNTQc and (d) ZnTNTQc, at 440 k magnification.

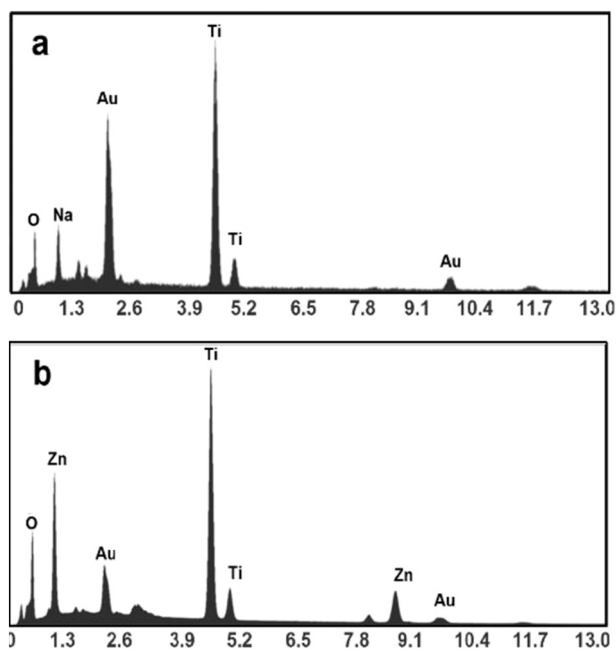


Fig. 2. EDS spectra of (a) NaTNT and (b) ZnTNT.

which are found on the nanotubes surface. The external diameters of the nanostructures are 9 ± 1 nm (NaTNT), 12 ± 5 nm (ZnTNT), 9 ± 2 nm (NaTNTQc) and 10 ± 1 nm (ZnTNTQc).

EDS analysis was used to confirm the exchange of sodium ions for zinc. Characteristic signals for titanium, oxygen and sodium atoms were observed in the NaTNT spectrum (Fig. 2a) and titanium, oxygen and zinc elements in the ZnTNT spectrum (Fig. 2b). These results indicate an effective exchange of sodium ions with the zinc present on the NaTNT surface, leading to the formation of ZnTNT.

The FTIR spectrum of NaTNT (Fig. 3a) show characteristic bands at: $3500\text{--}3200$ cm^{-1} , corresponding to the stretching vibration of the surface hydroxyl groups (Ti-OH), $1640\text{--}1630$ cm^{-1} , to the deformation of the OH bond of Ti-OH, and 892 cm^{-1} , to the vibrational mode of the Ti-O bond (nonbridging oxygen atoms coordinated with Na^+ ions), indicating the presence of sodium in the nanotubes [49,60,61]. The quercetin spectrum is similar to that reported in the literature [35,51], showing characteristic bands at: $3500\text{--}3200$ cm^{-1} , corresponding to the stretching vibration of the hydroxyl groups, 1660 cm^{-1} , to the carbonyl stretching vibration of aryl-ketone, $1600\text{--}1400$ cm^{-1} , to the vibration of the C=C bond of the aromatic ring, 1350 cm^{-1} , to the hydroxyl flexion vibration of the phenols, 1310 cm^{-1} , to the vibration of the C-H bond of the aromatic ring, and 1288 cm^{-1} , attributed to C-O stretching. In the NaTNTQc spectrum, the band at $3500\text{--}3000$ cm^{-1} is wider than that of the NaTNT spectrum. Additionally, two weak bands are present at 2941 and 2880 cm^{-1} , corresponding to the presence of aliphatic C-H bonds of quercetin. The wide band at 1630 cm^{-1} can be attributed to the overlapping bands at 1660 and 1600 cm^{-1} , representing the quercetin incorporated into the nanotubes, while the band at 892 cm^{-1} indicates the presence of sodium in the titanate nanotubes. This suggests that the composition of the NaTNT nanostructure remained unchanged even after the incorporation of quercetin. Other bands characteristic of quercetin can also be observed in the NaTNTQc spectrum, as well as slight displacement of the band at 1640 cm^{-1} , suggesting that the flavonoid was effectively incorporated into the NaTNT structure.

The FTIR spectrum of ZnTNT (Fig. 3c) exhibits the same bands found in the NaTNT spectrum, except for the band at 892 cm^{-1} attributed to the presence of sodium, indicating that the sodium ion exchange with zinc was effective [62]. Fig. 3d shows the ZnTNT and ZnTNTQc spectra, with characteristic quercetin bands in the ZnTNTQc

spectrum at 1740 cm^{-1} corresponding to the stretching vibration of C=O (quercetin), which interacts with the zinc atoms present in the ZnTNT structures [63]. These results are corroborated with other studies that observed the quercetin complexation with the zinc through the metal-carbonyl interaction of quercetin [64].

The crystallinity of NaTNT, ZnTNT, NaTNTQc and ZnTNTQc was analyzed by XRD (Fig. 3e). All the TNT nanostructures exhibited characteristic diffraction peaks at $2\theta = 10^\circ, 24^\circ, 28^\circ$ and 48° , corresponding to the crystalline planes of a typical $\text{M}_x\text{Ti}_3\text{O}_7$ structure. Applying the Bragg equation to the peak located at $2\theta = 10^\circ$ made it possible to obtain the interlamellar distance of the nanostructures ($0.87, 0.92, 0.88$ and 0.90 nm for NaTNT, NaTNTQc, ZnTNT and ZnTNTQc, respectively). The increase in interlamellar distance in the quercetin-coated nanostructures may be due to interaction between the flavonoid and the nanotubes [42,61]. In addition to the previously discussed peaks, ZnTNT showed diffraction peaks near $2\theta = 34^\circ$ and 36° , related to the formation of zinc oxide in the nanostructure [65]. The low intensity peak at $2\theta = 28^\circ$ compared to the peak at 24° indicates effective Na^+ ion exchange [66]. These results corroborate those obtained in EDS and FTIR analyses.

Thermogravimetric analysis (TGA) of NaTNT, NaTNTQc, ZnTNT, ZnTNTQc was carried out to estimate the amount of quercetin incorporated into the nanotubes and evaluate thermal stability. Fig. 4 compares the TG and DTG profiles of the nanostructures. Samples NaTNT and ZnTNT (Fig. 4a and b) exhibit two degradation steps attributed to absorbed ($40\text{--}100$ $^\circ\text{C}$) and interlayer water temperatures ($100\text{--}200$ $^\circ\text{C}$); as observed in previous studies by our group, these materials are thermally stable at higher temperatures [42,49]. The quercetin-coated nanotubes show a third degradation step ($200\text{--}400$ $^\circ\text{C}$ for NaTNTQc and $600\text{--}1000$ $^\circ\text{C}$ for ZnTNTQc), corresponding to quercetin degradation (Fig. 4c).

This displacement at higher temperatures in the third step of ZnTNTQc suggests a strong interaction between zinc and quercetin, corroborating the FTIR results. Other studies have also reported an increase in the thermal stability of quercetin-loaded nanostructures after zinc incorporation, suggesting a strong quercetin-Zn interaction that leads to the formation of complexes capable of stabilizing the flavonoid [34,35].

The amount of quercetin incorporated was estimated based on the difference in weight loss between 200 and 1000 $^\circ\text{C}$ of NaTNT or ZnTNT and NaTNTQc or ZnTNTQc, according to the method described in the literature [49]. Quercetin incorporation was around 12.5% for NaTNTQc and 27.7% for ZnTNTQc.

The *in vitro* release mechanism from nanoparticles involves two phases: (a) burst and (b) controlled release. In the first, flavonoid molecules are released from the nanostructure surface and in the second, via diffusion through the nanostructure. The second phase is associated with flavonoid-nanostructure interaction. In order to evaluate the influence of quercetin-nanostructure interaction on quercetin release, the *in vitro* release of NaTNTQc and ZnTNTQc in PBS was investigated ($\text{pH} = 5.5$). This medium was used to mimic the biological environment of cancer that would be encountered during diffusion towards the target cells.

Fig. 5 shows the quercetin release profiles of the NaTNTQc and ZnTNTQc nanostructures, with higher release values for NaTNT when compared to ZnTNT throughout the assay. After 6 h, approximately 44% of quercetin had been released in NaTNTQc and 10% in ZnTNTQc. Controlled release behavior was observed after 12 h. The diffusion-dependent phase showed that NaTNTQc released about 63% quercetin after 24 h, while only 18% was released in ZnTNTQc over the same period. Release remained constant after 48 h.

ZnTNTQc showed a slower release profile, suggesting that this nanostructure is better able to stabilize quercetin than NaTNTQc. This behavior may be associated with the difference between the nanostructures, where the presence of zinc on the surface causes quercetin complexation, resulting in stronger zinc-quercetin interaction. As such,

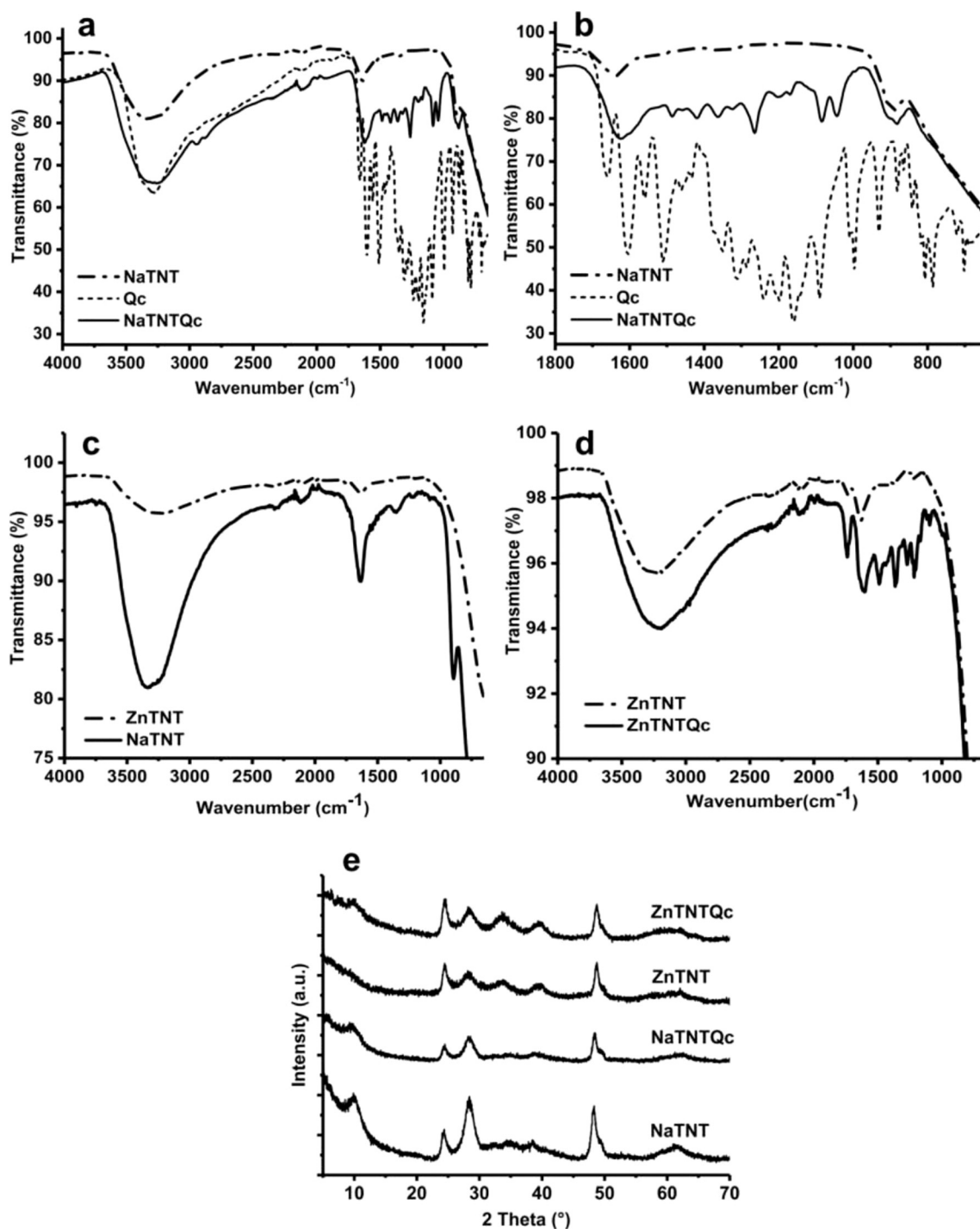


Fig. 3. FTIR spectra for (a) NaTNT, Qc and NaTNTQc, (b) 1800–650 cm^{-1} region, (c) NaTNT, ZnTNT, (d) comparison between ZnTNT and ZnTNTQc, (e) XRD patterns.

the ZnTNT nanostructure retains more of the flavonoid and releases it slowly. These results are consistent with the literature [51], which reported a similar quercetin release profile from silica nanoparticles in medium ($\text{pH} = 5.6$), with greater flavonoid release in the first 10 h. Similar findings were obtained for quercetin release (100%) from an SBA-15 silica matrix after 4 h [35]. Furthermore, flavonoid release was more controlled in zinc-modified SBA-15, indicating that zinc can delay quercetin release from silica nanoparticles or titanate nanotubes.

The cytotoxic effect of three new synthesized nanostructures (NaTNTQc, ZnTNT and ZnTNTQc) on the proliferation of T24 human bladder cancer cells and normal monkey kidney (Vero) cell lines was

assessed by MTT assay after 24 and 48 h. Quercetin and NaTNT were also evaluated for comparison purposes (Fig. 6).

As shown in Fig. 6 (a–d), Qc and NaTNT were considered non-cytotoxic to Vero cell viability. Furthermore, 100 and 200 $\mu\text{g}/\text{mL}$ of quercetin promoted a significant reduction in cell viability after 48 h of treatment (T24 cell viability). For NaTNT, the profile observed was considered non-cytotoxic in T24 cells for both times assessed. In addition, T24 cells treated with 50 and 100 $\mu\text{g}/\text{mL}$ of NaTNT increased mitochondrial metabolism in 24 and 48 h.

In contrast to the NaTNT profile, NaTNTQc, ZnTNT and ZnTNTQc exhibited different effects on cell viability. The results of the MTT assay

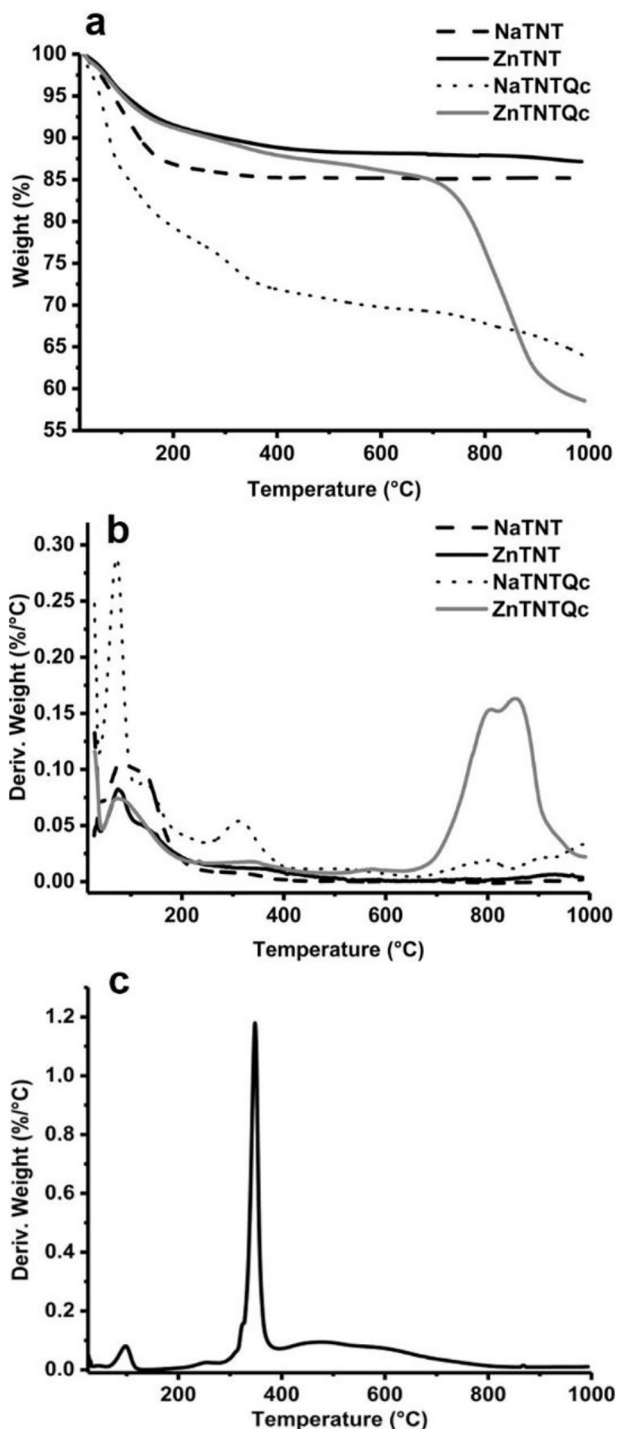


Fig. 4. (a) TG and (b) DTG curves of NaTNT, ZnTNT, NaTNTQc and ZnTNTQc. (c) DTG of Qc.

(Fig. 6e and f) showed that NaTNTQc promoted an increase in cell viability in the Vero lineage (200 $\mu\text{g}/\text{mL}$ at 24 h, and 50 to 200 $\mu\text{g}/\text{mL}$ at 48 h). Additionally, NaTNTQc reduced T24 cell viability at a concentration of 200 $\mu\text{g}/\text{mL}$ for both times tested. However, Vero and T24 cells treated with 200 $\mu\text{g}/\text{mL}$ ZnTNT showed decreased viability after 24 and 48 h (Fig. 6g and h). Moreover, greater mitochondrial metabolism was observed in Vero cells treated with 50 and 100 $\mu\text{g}/\text{mL}$ of ZnTNT after 48 h. ZnTNT also inhibited T24 cell viability at the highest concentrations (100 and 200 $\mu\text{g}/\text{mL}$) after 24 h. A significant inhibitory effect on T24 cells was also observed at 200 $\mu\text{g}/\text{mL}$ after 48 h. As shown

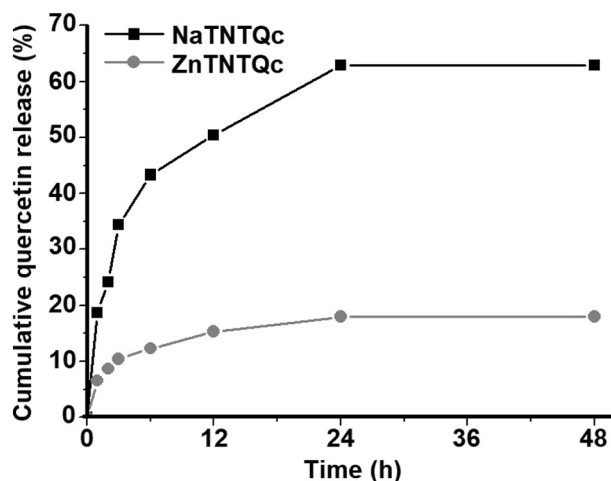


Fig. 5. Profiles for quercetin release from the NaTNTQc and ZnTNTQc nanostructures.

in Fig. 6 (i and j), ZnTNTQc promoted greater mitochondrial metabolism in Vero cells (25 and 100 $\mu\text{g}/\text{mL}$ after 48 h). For T24 cells, viability was inhibited after 24 h with 200 $\mu\text{g}/\text{mL}$ of ZnTNTQc and after 48 h with 50 to 200 $\mu\text{g}/\text{mL}$. However, this nanostructure was considered non-cytotoxic when compared with its precursor (ZnTNT) for both treatment times tested.

Previous studies have demonstrated the antiproliferative effect of quercetin on T24 cells [67]. Despite its recognized antitumor activity, the low bioavailability of quercetin is the main barrier to its use [68,69]. Cytotoxicity results suggest that quercetin coating on the titanate nanotubes significantly improved antitumoral action when compared with their precursors (without the flavonoid). This may be due to a synergistic effect in the quercetin-coated TNT nanostructures, since the oxidative characteristics of quercetin promote cell protection [70]. This effect is evident when comparing the viability of Vero cells treated with ZnTNT and ZnTNTQc (concentration of 200 $\mu\text{g}/\text{mL}$). Toxicity decreases with ZnTNTQc, suggesting it may be associated with the presence of Zn in the nanotubes (ZnTNT). Since quercetin interacts with the zinc atoms in the nanotubes (ZnTNTQc), as shown in FTIR analysis (Fig. 3), some atoms may no longer be available, thereby affecting their toxicity.

The cytotoxicity results of NaTNT and ZnTNT demonstrated that the nanostructures are stable and viable for quercetin coating as potential candidates for drug delivery due to their significant surface changes. These structures also showed greater selectivity for tumor cells, with potential application in biomedicine.

The biocompatibility of TNTs was investigated in Vero and T24 cells at four concentrations, ranging from 25 to 200 $\mu\text{g}/\text{mL}$. Few studies have investigated the cytotoxicity of TNT. According to Magrez et al., TiO_2 nanofilaments showed toxicity against H596 lung carcinoma cells at a concentration of 2 $\mu\text{g}/\text{mL}$ [45], while other authors reported no cytotoxicity in U87MG and SNB-19 glioblastoma cells [46,71], and that nanoparticle cytotoxicity is highly dependent on the cell type and morphology of the nanostructure [71,72]. In our study, TNTs were biocompatible after 2 days of exposure to Vero and T24 cells at a concentration of 200 $\mu\text{g}/\text{mL}$ for NaTNT, 50 times higher than the concentrations reported in the literature [45]. The other synthesized titanate nanostructures also showed biocompatibility in Vero and T24 cells at concentrations below 200 $\mu\text{g}/\text{mL}$. Based on the results obtained in the MTT assay, a non-cytotoxic dose (25 $\mu\text{g}/\text{mL}$ of TNTs) was chosen for subsequent experiments with T24 cell lines.

Since the nanostructure exhibited biocompatibility, bladder cancer cell internalization was evaluated. To our knowledge, few studies have investigated TNT internalization in cells. Some authors reported the internalization of titanate nanotubes in glioblastoma multiform cells

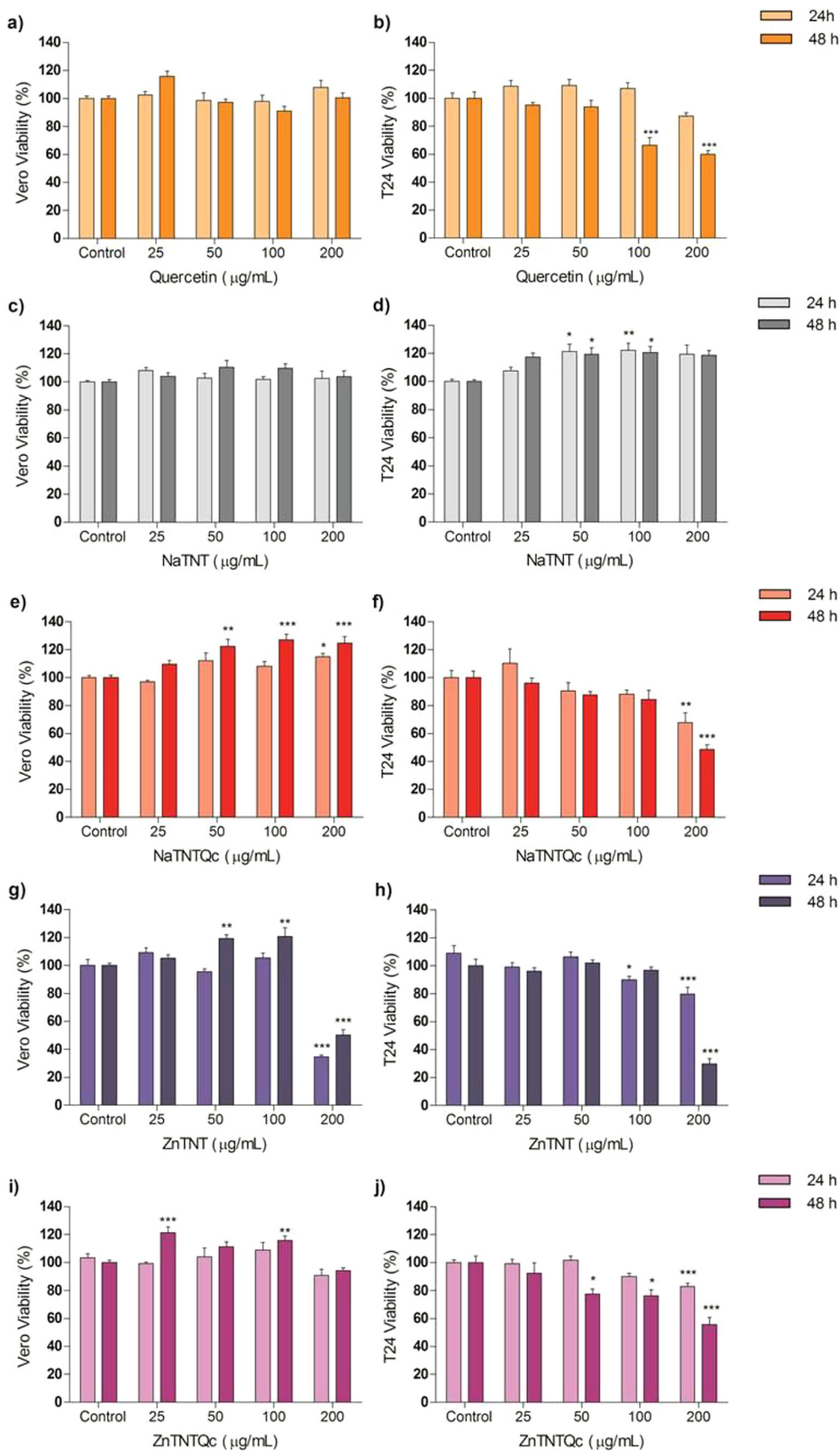


Fig. 6. Effect of (a-b) Qc, (c-d) NaTNT, (e-f) NaTNTQc, (g-h) ZnTNT, and (i-j) ZnTNTQc on the viability of Vero and T24 cell lines. At 80–90% confluence, cells were treated with the respective nanostructures (25, 50, 100, and 200 µg/mL) for 24 and 48 h. The data were analyzed for statistical significance using one-way ANOVA, followed by Tukey's post-hoc test. *** $p < 0.001$, ** $p < 0.01$, * $p < 0.05$.

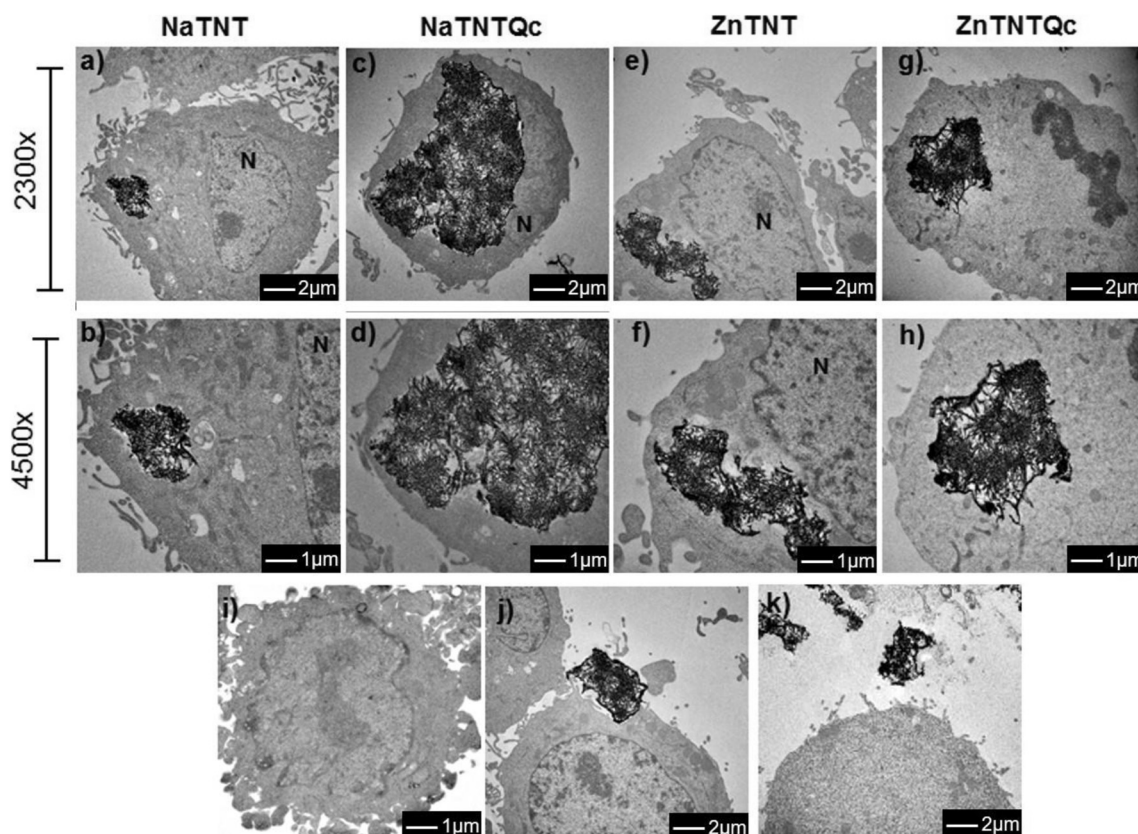


Fig. 7. TEM images of TNT incubated with T24 cells for 8 days: image (a-b) internalized NaTNT nanostructures found inside the cell. (c-d) high rate of NaTNTQc internalization. (e-f) ZnTNT found inside vesicles. (g-h) ZnTNTQc nanostructures detected in the cytosol. (i) control T24 cell. (j) internalization pathway observed (endocytosis). (k) nanostructures detected outside the cells, despite washing. The letter N indicates the nucleus.

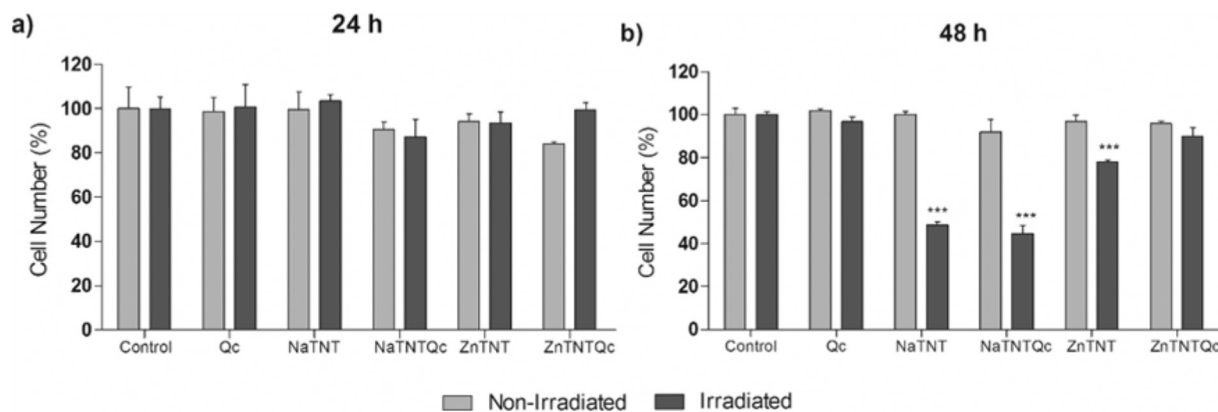


Fig. 8. Effect of TNTs on T24 cell proliferation. At 80–90% confluence, cells were treated with 25 $\mu\text{g}/\text{mL}$ of the respective nanostructures for 24 h (a) and 48 h (b). Next, one group was irradiated (5 Gy) and the other not (0 Gy). 24 h after irradiation, the cells were detached and counted. Controls were considered 100%. Data were analyzed for statistical significance by one-way ANOVA, followed by Tukey's post-hoc. *** $p < 0.001$.

[46,71]. In the present study, the internalization of NaTNT, NaTNTQc, ZnTNT and ZnTNTQc nanotubes was analyzed by TEM after 8 days of incubation (Fig. 7).

Following incubation, the T24 cells had internalized a significant number of nanotubes (Fig. 7c and e), while fewer had been internalized by other cells (Fig. 7a and g). Some nanotubes were also found inside the vesicles (Fig. 7d) or cytosol (Fig. 7g) of T24 cells. Endocytosis was observed in nanotubes internalization by tumor cells (Fig. 7j), as well as the presence of nanostructures outside the T24 cells, suggesting possible TNT exocytosis (Fig. 7l).

This study is the first to report the internalization of TNTs in T24 cells and our results indicate that internalization may be associated

with incubation time and TNT morphology. Indeed, the high concentration of TNT cells internalized may be related to the tubular morphology of the nanostructure and the length of time the cell is incubated with TNTs [71]. Titanate nanotubes with sodium were internalized by glioblastoma multiforme cells via different processes (endocytosis and diffusion) [46]. Baati et al. also reported TNT internalization by U87-MG cancer cells, after 1 h of incubation, and observed nanostructures inside vesicles or escaping from them into the cytosol [71]. Our results suggest that this is a continuous process, likely associated with the availability of TNTs in the extracellular environment. TEM images obtained after 8 days of incubation also demonstrate the biocompatibility of TNTs, evident in the normal morphology of the

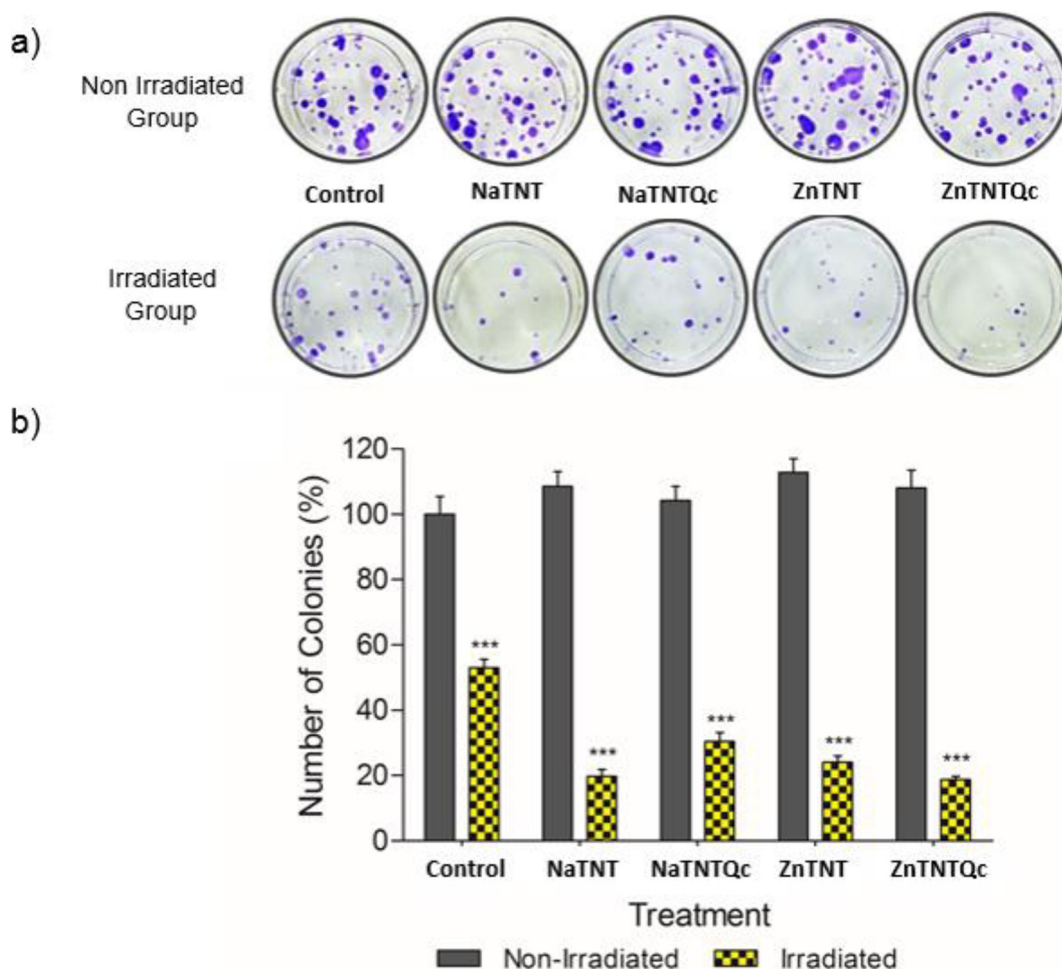


Fig. 9. Ability of T24 cells to form new colonies after treatment with 25 µg/mL of TNTs treatment with 5 Gy. A clonogenic assay was performed to assess the influence of TNT combined with irradiation on cell proliferation after 10 days. Evaluation of polyclonal cell population (a) and quantification of colony number (b). Each column represents the mean \pm SEM, *** $p < 0.001$, ** $p < 0.01$, and * $p < 0.05$, with results expressed in relation to control cells. All experiments were performed in triplicate.

nucleus during incubation when compared to control cells.

Ionizing radiation delivered during radiotherapy acts directly or indirectly, triggering a cascade of events (physical, chemical, biological and clinical) in cellular molecules and damaging DNA [73,74]. After exposure to ionizing radiation, energy transfer occurs, promoting the ionization and excitation of atoms and molecules (physicochemical effects). This triggers biological events such as cell death, causing irreparable DNA damage [75,76].

In this study, the biological response of T24 cells treated with quercetin and TNT was measured by cell counting (Fig. 8). As shown in Fig. 8, response differed at 24 and 48 h. Intracellular TNT concentrations may be related to the difference in cell number percentages at the two treatment times assessed. Baati et al. (2016) used ICP-MS to measure the intracellular concentration of TNTs after 1, 4, 24, 48 and 72 h of incubation with titanium nanotubes and found that intracellular titanium concentration increased from 1 to 48 h. In addition, TNT concentration was practically the same at 72 and 48 h, suggesting possible cell saturation by TNTs [71]. For T24 cells treated with 25 µg/mL of quercetin or nanostructures (NaTNT, NaTNTQc, ZnTNT and ZnTNTQc) and incubated for 24 h, there was no significant variation in the number of cells between irradiated and nonirradiated groups (Fig. 8a); however, intergroup differences in cell number were observed in T24 cells treated under the same conditions and incubated for 48 h. NaTNT, NaTNTQc and ZnTNT promoted a significant decrease on the number of irradiated T24 cells (Fig. 8b). These results are similar to those reported in the

literature, indicating that sodium titanate nanotubes reduced the number of glioblastoma cells when associated with radiotherapy [46]. The response profiles of ZnTNT and ZnTNTQc also differed from those obtained for sodium titanate nanotubes. As shown in Fig. 8b, 25 µg/mL of ZnTNT combined with irradiation reduced the number of cells in the T24 cell line, which did not occur for ZnTNTQc 48 h after irradiation.

These results can be explained by several factors that influence biological response, such as linear energy transfer, dose and treatment time [76,77]. The dose was fixed at 5 Gy, while the incubation time with the TNT varied. Incubation time is directly related to the rate of TNT internalization by the T24 cells. The TNT internalization rate changed in cells treated for 24 h or 48 h [71], which could explain the possible difference in cell numbers between the irradiated groups (24 and 48 h). Since the amount of energy deposited by gamma ray is relatively small [76], TNTs may indirectly absorb ionizing radiation and deliver the energy over time. Additionally, the rate of internalization increased up to 48 h, drastically reducing the number of living cells. These results suggest that the incubation time of TNTs is a crucial parameter in the radiosensitization process.

It is also important to note that nanotube structure may also be associated with the behavior profile of the cells. Comparison of Fig. 8a and b shows that the chemical nature of the nanostructures may influence the treatment response when combined with radiation. Both titanate nanotubes with sodium exhibited a reduction in the number of cells, whereas only ZnTNT showed the same inhibitory profile.

However, other parameters should also be taken into account, such as controlled flavonoid release and the rate of nanostructure internalization.

Cell death refers to the irreversible cessation of vital functions (loss of clonogenic integrity and ability to proliferate indefinitely) [78,79]. Since cell numbers did not decline in the 24 h cell group, these cells were selected for 48 h incubation and exposed to radiation for the subsequent experiments. The proliferative effect on TNT-treated T24 cells was measured by clonogenic assay after 48 h of TNT cell incubation (Fig. 9). The results indicated a significant decrease in proliferative capacity for T24 cell lines exposed to TNT combined with irradiation. As such, only the cytotoxic effect of ionizing radiation was evaluated, comparing the nonirradiated and irradiated groups, with controls from the nonirradiated group (0 Gy) corresponding to 100% survival.

Cytotoxicity was also assessed for each treatment condition when compared to the group irradiated through inhibition of colony formation. Ten days after treatment with NaTNT, NaTNTQc and ZnTNT following irradiation, there was a significant decline in the number of polyclonal colonies and their diameter in relation to controls (Fig. 9a). Moreover, ZnTNTQc showed no antiproliferative effect on cell number, but significantly inhibited the number of T24 colonies.

The effect of nanostructures radiosensitization was observed in both experimental groups, with a significant decrease in the number of T24 colonies formed (Fig. 9a, b). This effect of radiosensitization by the reduction of clonogenic integrity was previously reported in the literature [80–83].

Moreover, the number of colonies formed is substantially lower when the results between each treatment condition of the irradiated group are compared with those of the respective controls (Fig. 9b). These findings are similar to those reported in the literature, whereby sodium titanate nanotubes interrupted the cell cycle of glioblastomas through the production of ROS (reactive oxygen species) [46]. Furthermore, studies indicate that nanoparticle internalization may activate cellular autophagy (removal of unnecessary or dysfunctional components) in response to the stress caused by cell adaptation to the internalized structure [46,84,85]. Thus, the increase in the effect of cellular radiosensitization observed here may have occurred due to nanostructure internalization by T24 cells before irradiation.

Another relevant aspect may have influenced the results obtained by ZnTNT and ZnTNTQc is the presence of the zinc ion, which may interact with γ radiation (photoelectric effect). Previous studies have demonstrated that ZnFe₂O₄ nanoparticles can not only increase the efficiency of radiotherapy, but are also easily separated from the cell environment via an external magnetic field after radiotherapy [86]. Although the tests conducted here answer the initial questions, further research is needed to elucidate the mechanisms of action. Based on the results obtained here, the nanostructures studied reduced the survival of tumor cells and may be a promising tool in the future treatment of bladder cancer.

4. Conclusion

In this study, new hybrid nanostructures based on sodium and zinc titanate nanotubes coated with quercetin were successfully synthesized. Thermogravimetric analysis showed strong interaction between Qc and ZnTNT, used as support, while FTIR indicated possible interaction between Zn atoms and the flavonoid. The nanostructures synthesized in this study showed biocompatibility with the concentrations used and time. The *in vitro* results of internalization assays demonstrated that TNT (NaTNT, NaTNTQc, ZnTNT and ZnTNTQc) can penetrate human bladder cancer cells and remain in the cytosol for 8 days, with no signs of cytotoxicity. These results suggest that TNTs increased the effectiveness of *in vitro* radiotherapy in T24 cells. The development of these TNTs may constitute a new tool in bladder cancer research and clinical therapy.

Acknowledgements

This study was partially funded by the Coordenação de Aperfeiçoamento de Pessoal de Nível Superior – Brasil (CAPES) – Finance Code 001. The authors would like to thank CAPES and CNPq for the scholarships awarded, and FAPERGS and PUCRS for their financial and technical support. We are also grateful to the PUCRS Central Laboratory of Microscopy and Microanalysis (LabCEMM) for the FESEM and TEM analyses.

References

- [1] J. Ferlay, E. Steliarova-Foucher, J. Lortet-Tieulent, S. Rosso, J.W.W. Coebergh, H. Comber, D. Forman, F. Bray, Reprint of: cancer incidence and mortality patterns in Europe: estimates for 40 countries in 2012, *Eur. J. Cancer* 49 (2013) 1374–1403, <https://doi.org/10.1016/j.ejca.2015.05.004>.
- [2] S. Antoni, J. Ferlay, I. Soerjomataram, A. Znaor, A. Jemal, F. Bray, Bladder cancer incidence and mortality: a global overview and recent trends, *Eur. Urol.* 71 (2017) 96–108, <https://doi.org/10.1016/j.euro.2016.06.010>.
- [3] H. Moch, A.L. Cubilla, P.A. Humphrey, V.E. Reuter, T.M. Ulbright, The 2016 WHO classification of tumours of the urinary system and male genital organs—part a: renal, penile, and testicular tumours, *Eur. Urol.* 70 (2016) 93–105, <https://doi.org/10.1016/j.euro.2016.02.029>.
- [4] J.H. Buss, K.R. Beghini, C.B. Bender, A.R. Pohlmann, S.S. Guterres, T. Collares, F.K. Seixas, Nano-BCG: a promising delivery system for treatment of human bladder cancer, *Front. Pharmacol.* 8 (2018) 1–9, <https://doi.org/10.3389/fphar.2017.00977>.
- [5] J. Bellmunt, D.P. Petrylak, New therapeutic challenges in advanced bladder cancer, *Semin. Oncol.* 39 (2012) 598–607, <https://doi.org/10.1053/j.seminoncol.2012.08.007>.
- [6] R.M. Bambury, J.E. Rosenberg, Advanced urothelial carcinoma: overcoming treatment resistance through novel treatment approaches, *Front. Pharmacol.* 4 (2013) 1–7, <https://doi.org/10.3389/fphar.2013.00003>.
- [7] J.E. Jacobs, B.L., Lee, C.T., Montie, Bladder cancer in 2010, *CA Cancer J. Clin.* 60 (2010) 244–272. doi:<https://doi.org/10.3322/caac.20077>. Available.
- [8] C.M. Russell, A.H. Lebastchi, T. Borza, D.E. Spratt, T.M. Morgan, The role of transurethral resection in trimodal therapy for muscle-invasive bladder cancer, *Bl. Cancer.* 2 (2016) 381–394, <https://doi.org/10.3233/BLC-160076>.
- [9] A.M. Kamat, N.M. Hahn, J.A. Efsthathiou, S.P. Lerner, P.U. Malmström, W. Choi, C.C. Guo, Y. Lotan, W. Kassouf, Bladder cancer, *Lancet* 388 (2016) 2796–2810, [https://doi.org/10.1016/S0140-6736\(16\)30512-8](https://doi.org/10.1016/S0140-6736(16)30512-8).
- [10] C.J. Down, R. Nair, R. Thurairaja, Bladder cancer, *Surg. (United Kingdom)*. 34 (2016) 532–539, <https://doi.org/10.1016/j.mpsur.2016.08.001>.
- [11] S.R. Shukla, K.S. Kulkarni, Depolymerization of poly(ethylene terephthalate) waste, *J. Appl. Polym. Sci.* 85 (2002) 1765–1770, <https://doi.org/10.1002/app.10714>.
- [12] F. Dietrich, F. Figueiró, E.C. Filippi-Chiela, A.R. Cappellari, L. Rockenbach, A. Tremblay, P.B. de Paula, R. Roesler, A.B. Filho, J. Sévigny, F.B. Morrone, A.M.O. Battastini, Ecto-5'-nucleotidase/CD73 contributes to the radiosensitivity of T24 human bladder cancer cell line, *J. Cancer Res. Clin. Oncol.* 144 (2018) 469–482, <https://doi.org/10.1007/s00432-017-2567-3>.
- [13] M. Roy Chowdhury, C. Schumann, D. Bhakta-Guha, G. Guha, Cancer nanotheranostics: strategies, promises and impediments, *Biomed. Pharmacother.* 84 (2016) 291–304, <https://doi.org/10.1016/j.biopha.2016.09.035>.
- [14] R. Li, B. Liu, J. Gao, The application of nanoparticles in diagnosis and theranostics of gastric cancer, *Cancer Lett.* 386 (2017) 123–130, <https://doi.org/10.1016/j.canlet.2016.10.032>.
- [15] A. Pugazhendhi, T.N.J.I. Edison, I. Karuppusamy, B. Kathirvel, Inorganic nanoparticles: a potential cancer therapy for human welfare, *Int. J. Pharm.* 539 (2018) 104–111, <https://doi.org/10.1016/j.ijpharm.2018.01.034>.
- [16] A. Khan, A.A.P. Khan, A.M. Asiri, M.A. Rub, M.M. Rahman, S.A. Ghani, *In vitro* studies of carbon fiber microbiosensor for dopamine neurotransmitter supported by copper-graphene oxide composite, *Microchim. Acta* 181 (2014) 1049–1057, <https://doi.org/10.1007/s00604-014-1202-0>.
- [17] A. Khan, A.A.P. Khan, A.M. Asiri, K.A. Alamry, Preparation and characterization of hybrid graphene oxide composite and its application in paracetamol microbiosensor, *Polym. Compos.* 36 (2015) 221–228, <https://doi.org/10.1002/pc.23981>.
- [18] A. Khan, A.A.P. Khan, A.M. Asiri, Toward design and measurement of electrical conductivity and thermal properties of silver nanoparticle embedded poly(o-anisidine) molybdophosphate nanocomposite and its application as microbiosensor, *Polym. Compos.* 38 (2017) E237–E245, <https://doi.org/10.1002/pc.23981>.
- [19] A. Khan, A.A.P. Khan, A.M. Asiri, M.A. Rub, N. Azum, M.M. Rahman, S.B. Khan, S.A. Ghani, A new trend on biosensor for neurotransmitter choline/acetylcholine - an overview, *Appl. Biochem. Biotechnol.* 169 (2013) 1927–1939, <https://doi.org/10.1007/s12010-013-0099-0>.
- [20] M. Li, F. Zhang, Y. Su, J. Zhou, W. Wang, Nanoparticles designed to regulate tumor microenvironment for cancer therapy, *Life Sci.* 201 (2018) 37–44, <https://doi.org/10.1016/j.lfs.2018.03.044>.
- [21] G. Baskar, B.G. Garrick, K. Lalitha, M. Chamundeswari, Gold nanoparticle mediated delivery of fungal asparaginase against cancer cells, *J. Drug Deliv. Sci. Technol.* 44 (2018) 498–504, <https://doi.org/10.1016/j.jddst.2018.02.007>.
- [22] Y. Ju, B. Dong, J. Yu, Y. Hou, Inherent multifunctional inorganic nanomaterials for imaging-guided cancer therapy, *Nano Today* 26 (2019) 108–122, <https://doi.org/>

- 10.1016/j.nantod.2019.03.006.
- [23] Y. Pan, P. Xue, S. Liu, L. Zhang, Q. Guan, J. Zhu, X. Tian, Metal-based hybrid nanoparticles as radiosensitizers in cancer therapy, *Colloids Interface Sci. Commun.* 23 (2018) 45–51, <https://doi.org/10.1016/j.colcom.2018.01.004>.
- [24] Y. Chang, L. He, Z. Li, L. Zeng, Z. Song, P. Li, L. Chan, Y. You, X.F. Yu, P.K. Chu, T. Chen, Designing core-shell gold and selenium nanocomposites for cancer radiochemotherapy, *ACS Nano* 11 (2017) 4848–4858, <https://doi.org/10.1021/acsnano.7b01346>.
- [25] Y. Yong, X. Cheng, T. Bao, M. Zu, L. Yan, W. Yin, C. Ge, D. Wang, Z. Gu, Y. Zhao, Tungsten sulfide quantum dots as multifunctional nanotheranostics for in vivo dual-modal image-guided photothermal/radiotherapy synergistic therapy, *ACS Nano* 9 (2015) 12451–12463, <https://doi.org/10.1021/acsnano.5b05825>.
- [26] J. Du, X. Zheng, Y. Yong, J. Yu, X. Dong, C. Zhang, R. Zhou, B. Li, L. Yan, C. Chen, Z. Gu, Y. Zhao, Design of TPGS-functionalized Cu₃BiS₃ nanocrystals with strong absorption in the second near-infrared window for radiation therapy enhancement, *Nanoscale* 9 (2017) 8229–8239, <https://doi.org/10.1039/c7nr02213a>.
- [27] S.H. Thilakarathna, H.P. Vasantha Rupasinghe, Flavonoid bioavailability and attempts for bioavailability enhancement, *Nutrients* 5 (2013) 3367–3387, <https://doi.org/10.3390/nu5093367>.
- [28] D. Teekaraman, S.P. Elayapillai, M.P. Viswanathan, A. Jagadeesan, Quercetin inhibits human metastatic ovarian cancer cell growth and modulates components of the intrinsic apoptotic pathway in PA-1 cell line, *Chem. Biol. Interact.* 300 (2019) 91–100, <https://doi.org/10.1016/j.cbi.2019.01.008>.
- [29] N.S. Srivastava, R.A.K. Srivastava, Curcumin and quercetin synergistically inhibit cancer cell proliferation in multiple cancer cells and modulate Wnt/ β -catenin signaling and apoptotic pathways in A375 cells, *Phytomedicine* 52 (2019) 117–128, <https://doi.org/10.1016/j.phymed.2018.09.224>.
- [30] K. Wang, R. Liu, J. Li, J. Mao, Y. Lei, J. Wu, J. Zeng, T. Zhang, H. Wu, L. Chen, C. Huang, Y. Wei, Quercetin induces protective autophagy in gastric cancer cells: involvement of Akt-mTOR- and hypoxia-induced factor 1 α -mediated signaling, *Autophagy* 7 (2011) 966–978, <https://doi.org/10.4161/autophagy.7.9.15863>.
- [31] S. Borska, M. Chmielewska, T. Wysocka, M. Drag-Zalesinska, M. Zabel, P. Dziegiel, In vitro effect of quercetin on human gastric carcinoma: targeting cancer cells death and MDR, *Food Chem. Toxicol.* 50 (2012) 3375–3383, <https://doi.org/10.1016/j.fct.2012.06.035>.
- [32] C.S. Lei, Y.C. Hou, M.H. Pai, M.T. Lin, S.L. Yeh, Effects of quercetin combined with anticancer drugs on metastasis-associated factors of gastric cancer cells: *in vitro* and *in vivo* studies, *J. Nutr. Biochem.* 51 (2018) 105–113, <https://doi.org/10.1016/j.jnutbio.2017.09.011>.
- [33] C.M. Nday, E. Halevas, G.E. Jackson, A. Salifoglou, Quercetin encapsulation in modified silica nanoparticles: potential use against Cu(II)-induced oxidative stress in neurodegeneration, *J. Inorg. Biochem.* 145 (2015) 51–64, <https://doi.org/10.1016/j.jinorgbio.2015.01.001>.
- [34] M. Popova, I. Trendafilova, A. Szegedi, J. Mihály, P. Németh, S.G. Marinova, H.A. Aleksandrov, G.N. Vayssilov, Experimental and theoretical study of quercetin complexes formed on pure silica and Zn-modified mesoporous MCM-41 and SBA-16 materials, *Microporous Mesoporous Mater.* 228 (2016) 256–265, <https://doi.org/10.1016/j.micromeso.2016.04.001>.
- [35] I. Trendafilova, A. Szegedi, J. Mihály, G. Momekov, N. Lihareva, M. Popova, Preparation of efficient quercetin delivery system on Zn-modified mesoporous SBA-15 silica carrier, *Mater. Sci. Eng. C* 73 (2017) 285–292, <https://doi.org/10.1016/j.msec.2016.12.063>.
- [36] Á. Kukovec, K. Kordás, J. Kiss, Z. Kónya, Atomic scale characterization and surface chemistry of metal modified titanate nanotubes and nanowires, *Surf. Sci. Rep.* 71 (2016) 473–546, <https://doi.org/10.1016/j.surfrep.2016.06.001>.
- [37] D.V. Bavykin, B.A. Cressey, M.E. Light, F.C. Walsh, An aqueous, alkaline route to titanate nanotubes under atmospheric pressure conditions, *Nanotechnology* 19 (2008), <https://doi.org/10.1088/0957-4484/19/27/275604>.
- [38] G.R. Lima, W.F. Monteiro, R. Ligabue, R.M.C. Santana, Titanate nanotubes as new nanostructured catalyst for depolymerization of PET by glycolysis reaction, *Mater. Res.* 20 (2017) 588–595, <https://doi.org/10.1590/1980-5373-mr-2017-0645>.
- [39] M.E. Martínez-Klimov, P. Hernández-Hipólito, M. Martínez-García, T.E. Klimova, Pd catalysts supported on hydrogen titanate nanotubes for Suzuki-Miyaura cross-coupling reactions, *Catal. Today* 305 (2018) 58–64, <https://doi.org/10.1016/j.cattod.2017.10.015>.
- [40] W.F. Monteiro, M.O. Vieira, C.O. Calgario, O.W. Perez-Lopez, R.A. Ligabue, Dry reforming of methane using modified sodium and protonated titanate nanotube catalysts, *Fuel* 253 (2019) 713–721, <https://doi.org/10.1016/j.fuel.2019.05.019>.
- [41] A.A.C. Pereira, R.R. Santos, J.R.M. d'Almeida, Effects of incorporating titanate nanotubes on the mechanical properties of polyamide 11, *Polym. Test.* 68 (2018) 238–247, <https://doi.org/10.1016/j.polymertesting.2018.04.019>.
- [42] W.F. Monteiro, C.A.B. Santos, M.S. Hoffmann, C.L.P. Carone, S.M.O. Einloft, M.O. De Souza, R.A. Ligabue, Modified titanate nanotubes for the production of novel aliphatic polyurethane nanocomposites, *Polym. Compos.* (2018) 1–9, <https://doi.org/10.1002/pc.25038>.
- [43] B. Joshi, C. Regmi, D. Dhakal, G. Gyawali, S.W. Lee, Efficient inactivation of *Staphylococcus aureus* by silver and copper loaded photocatalytic titanate nanotubes, *Prog. Nat. Sci. Mater. Int.* 28 (2018) 15–23, <https://doi.org/10.1016/j.pnsc.2018.01.004>.
- [44] F. Sallem, J. Boudon, O. Heintz, I. Séverin, A. Megriche, N. Millot, Synthesis and characterization of chitosan-coated titanate nanotubes: towards a new safe nano-carrier, *Dalton Trans.* 46 (2017) 15386–15398, <https://doi.org/10.1039/c7dt03029k>.
- [45] A. Magrez, L. Horvth, R. Smajda, V. Salicio, N. Pasquier, L. Forr, B. Schwaller, Cellular toxicity of TiO₂-based nanofilaments, *ACS Nano* 3 (2009) 2274–2280, <https://doi.org/10.1021/nn9002067>.
- [46] C. Mirjole, A.L. Papa, G. Créhange, O. Raguin, C. Seignez, C. Paul, G. Truc, P. Maingon, N. Millot, The radiosensitization effect of titanate nanotubes as a new tool in radiation therapy for glioblastoma: a proof-of-concept, *Radiother. Oncol.* 108 (2013) 136–142, <https://doi.org/10.1016/j.radonc.2013.04.004>.
- [47] S. Sruthi, A. Loiseau, J. Boudon, F. Sallem, L. Maurizi, P.V. Mohanan, G. Lizard, N. Millot, *In vitro* interaction and biocompatibility of titanate nanotubes with microglial cells, *Toxicol. Appl. Pharmacol.* 353 (2018) 74–86, <https://doi.org/10.1016/j.taap.2018.06.013>.
- [48] W.F. Monteiro, C.A.B. dos Santos, S. Einloft, M. Oberson, C.L.P. Carone, R.A. Ligabue, Preparation of modified titanate nanotubes and its application in polyurethane nanocomposites, *Macromol. Symp.* 368 (2016) 93–97, <https://doi.org/10.1002/masy.201500146>.
- [49] W.F. Monteiro, M.O. Vieira, A.S. Aquino, M.O. de Souza, J. de Lima, S. Einloft, R. Ligabue, CO₂ conversion to propylene carbonate catalyzed by ionic liquid containing organosilane groups supported on titanate nanotubes/nanowires, *Appl. Catal. A Gen.* 544 (2017) 46–54, <https://doi.org/10.1016/j.apcata.2017.07.011>.
- [50] S. Thennarasu, K. Rajasekar, K. Balkis Ameen, Hydrothermal temperature as a morphological control factor: preparation, characterization and photocatalytic activity of titanate nanotubes and nanoribbons, *J. Mol. Struct.* 1049 (2013) 446–457, <https://doi.org/10.1016/j.molstruc.2013.06.064>.
- [51] A. Sarkar, S. Ghosh, S. Chowdhury, B. Pandey, P.C. Sil, Targeted delivery of quercetin loaded mesoporous silica nanoparticles to the breast cancer cells, *Biochim. Biophys. Acta, Gen. Subj.* 1860 (2016) 2065–2075, <https://doi.org/10.1016/j.bbagen.2016.07.001>.
- [52] N.F. Nicoletti, T.C. Erig, R.F. Zanin, M.R. Roxo, N.P. Ferreira, M.V. Gomez, F.B. Morrone, M.M. Campos, Pre-clinical evaluation of voltage-gated calcium channel blockers derived from the spider *P. nigriventer* in glioma progression, *Toxicol.* 129 (2017) 58–67, <https://doi.org/10.1016/j.toxicol.2017.02.001>.
- [53] L. Rockenbach, L. Bavareco, P. Fernandes Farias, A.R. Cappellari, C.H. Barrios, F. Bueno Morrone, A.M. Oliveira Battastini, Alterations in the extracellular catabolism of nucleotides are involved in the antiproliferative effect of quercetin in human bladder cancer T24 cells, *Urol. Oncol. Semin. Orig. Investig.* 31 (2013) 1204–1211, <https://doi.org/10.1016/j.urolonc.2011.10.009>.
- [54] C.-N. Im, B.M. Kim, E.-Y. Moon, D.-W. Hong, J.W. Park, S.H. Hong, Characterization of H460R, a radioresistant human lung cancer cell line, and involvement of syn-trophin beta 2 (SNTB2) in radioresistance, *Genomics Inform* 11 (2013) 245, <https://doi.org/10.5808/GI.2013.11.4.245>.
- [55] S.N. Sunil Gowda, S. Rajasowmiya, V. Vadivel, S. Banu Devi, A. Celestin Jerald, S. Marimuthu, N. Devipriya, Gallic acid-coated silver nanoparticle alters the expression of radiation-induced epithelial-mesenchymal transition in non-small lung cancer cells, *Toxicol. In Vitro* 52 (2018) 170–177, <https://doi.org/10.1016/j.tiv.2018.06.015>.
- [56] R. Chan, P. Sethi, A. Jyoti, R. McGarry, M. Upreti, Investigating the radioresistant properties of lung cancer stem cells in the context of the tumor microenvironment, *Radiat. Res.* 185 (2016) 169–181, <https://doi.org/10.1667/RR14285.1>.
- [57] T.M.F. Marques, O.P. Ferreira, J.A.P. Da Costa, K. Fujisawa, M. Terrones, B.C. Viana, Study of the growth of CeO₂ nanoparticles onto titanate nanotubes, *J. Phys. Chem. Solids* 87 (2015) 213–220, <https://doi.org/10.1016/j.jpcs.2015.08.022>.
- [58] X. Yang, L. Wu, L. Ma, X. Li, T. Wang, S. Liao, Pd nano-particles (NPs) confined in titanate nanotubes (TNTs) for hydrogenation of cinnamaldehyde, *Catal. Commun.* 59 (2015) 184–188, <https://doi.org/10.1016/j.catcom.2014.10.031>.
- [59] C.C. Tsai, L.C. Chen, T.F. Yeh, H. Teng, In situ Sn²⁺ incorporation synthesis of titanate nanotubes for photocatalytic dye degradation under visible light illumination, *J. Alloys Compd.* 546 (2013) 95–101, <https://doi.org/10.1016/j.jallcom.2012.08.081>.
- [60] W. Linghu, Y. Sun, H. Yang, K. Chang, G. Sheng, T. Hayat, N.S. Alharbi, J. Ma, Macroscopic and spectroscopic exploration on the removal performance of titanate nanotubes towards Zn(II), *J. Mol. Liq.* 244 (2017) 146–153, <https://doi.org/10.1016/j.molliq.2017.08.126>.
- [61] G. Niu, W. Liu, T. Wang, J. Ni, Adsorption of Cr(VI) onto amino-modified titanate nanotubes using 2-bromoethylamine hydrobromide through SN2 reaction, *J. Colloid Interface Sci.* 401 (2013) 133–140, <https://doi.org/10.1016/j.jcis.2013.03.037>.
- [62] T. Wang, W. Liu, N. Xu, J. Ni, Adsorption and desorption of Cd(II) onto titanate nanotubes and efficient regeneration of tubular structures, *J. Hazard. Mater.* 250–251 (2013) 379–386, <https://doi.org/10.1016/j.jhazmat.2013.02.016>.
- [63] T.V. Surendra, S.M. Roopan, N.A. Al-Dhabi, M.V. Arasu, G. Sarkar, K. Suthindhiran, Vegetable peel waste for the production of ZnO nanoparticles and its toxicological efficiency, antifungal, hemolytic, and antibacterial activities, *Nanoscale Res. Lett.* 11 (2016) 1–10, <https://doi.org/10.1186/s11671-016-1750-9>.
- [64] J. Tan, B. Wang, L. Zhu, DNA binding, cytotoxicity, apoptotic inducing activity, and molecular modeling study of quercetin zinc(II) complex, *Bioorg. Med. Chem.* 17 (2009) 614–620, <https://doi.org/10.1016/j.bmc.2008.11.063>.
- [65] L.S. Wang, M.W. Xiao, X.J. Huang, Y.D. Wu, Synthesis, characterization, and photocatalytic activities of titanate nanotubes surface-decorated by zinc oxide nanoparticles, *J. Hazard. Mater.* 161 (2009) 49–54, <https://doi.org/10.1016/j.jhazmat.2008.03.080>.
- [66] S.R.A. Santos, I.S. Jardim, H.A. Bicalho, I. Binatti, E.M.B. Sousa, A.M. Peres, R.R. Resende, E. Lorençon, Multifunctional catalysts based on carbon nanotubes and titanate nanotubes for oxidation of organic compounds in biphasic systems, *J. Colloid Interface Sci.* 483 (2016) 211–219, <https://doi.org/10.1016/j.jcis.2016.08.025>.
- [67] L. Ma, J.M. Feugang, P. Konarski, J. Wang, J. Lu, S. Fu, B. Ma, B. Tian, C. Zou, Z. Wang, Growth inhibitory effects of quercetin on bladder cancer cell, *Front. Biosci.* 11 (2006) 2275, <https://doi.org/10.2741/1970>.

- [68] P. Sadhukhan, M. Kundu, S. Chatterjee, N. Ghosh, P. Manna, J. Das, P.C. Sil, Targeted delivery of quercetin via pH-responsive zinc oxide nanoparticles for breast cancer therapy, *Mater. Sci. Eng. C* 100 (2019) 129–140, <https://doi.org/10.1016/j.msec.2019.02.096>.
- [69] W. Wang, C. Sun, L. Mao, P. Ma, F. Liu, J. Yang, Y. Gao, The biological activities, chemical stability, metabolism and delivery systems of quercetin: a review, *Trends Food Sci. Technol.* 56 (2016) 21–38, <https://doi.org/10.1016/j.tifs.2016.07.004>.
- [70] C. Bonechi, A. Donati, G. Tamasi, G. Leone, M. Consumi, C. Rossi, S. Lamponi, A. Magnani, Protective effect of quercetin and rutin encapsulated liposomes on induced oxidative stress, *Biophys. Chem.* 233 (2018) 55–63, <https://doi.org/10.1016/j.bpc.2017.11.003>.
- [71] T. Baati, B.B. Kefi, A. Aouane, L. Njim, F. Chaspoul, V. Heresanu, A. Kerkeni, F. Neffati, M. Hammami, Biocompatible titanate nanotubes with high loading capacity of genistein: cytotoxicity study and anti-migratory effect on U87-MG cancer cell lines, *RSC Adv.* 6 (2016) 101688–101696, <https://doi.org/10.1039/c6ra24569b>.
- [72] B. L'Azou, J. Jorly, D. On, E. Sellier, F. Moisan, J. Fleury-Feith, J. Cambar, P. Brochard, C. Ohayon-Courtès, *In vitro* effects of nanoparticles on renal cells, *Part. Fibre Toxicol.* 5 (2008) 22, <https://doi.org/10.1186/1743-8977-5-22>.
- [73] L. Ollivier, A.R. Padhani, J. Leclère, International criteria for measurement of tumour response, *Cancer Imaging* 2 (2001) 31–39, <https://doi.org/10.1102/1470-7330.2001.017>.
- [74] E.J. Hall, Cancer caused by x-rays—a random event? *Lancet Oncol.* 8 (2007) 369–370, [https://doi.org/10.1016/S1470-2045\(07\)70113-4](https://doi.org/10.1016/S1470-2045(07)70113-4).
- [75] B.M. Fenton, E.M. Lord, S.F. Paoni, Effects of radiation on tumor intravascular oxygenation, vascular configuration, development of hypoxia, and clonogenic survival, *Radiat. Res.* 155 (2001) 360–368, [https://doi.org/10.1667/0033-7587\(2001\)155\[0360:EOROTI\]2.0.CO;2](https://doi.org/10.1667/0033-7587(2001)155[0360:EOROTI]2.0.CO;2).
- [76] R. Baskar, J. Dai, N. Wenlong, R. Yeo, K.-W. Yeoh, Biological response of cancer cells to radiation treatment, *Front. Mol. Biosci.* 1 (2014) 1–9, <https://doi.org/10.3389/fmols.2014.00024>.
- [77] I.V. Mavragani, D.A. Laskaratou, B. Frey, S.M. Candéias, U.S. Gaipl, K. Lumniczky, A.G. Georgakilas, Key mechanisms involved in ionizing radiation-induced systemic effects. A current review, *Toxicol. Res. (Camb.)* 5 (2015) 12–33, <https://doi.org/10.1039/c5tx00222b>.
- [78] L.E. Dillehay, A Model of Cell Killing by Low-dose-rate Radiation Including Repair of Sublethal Damage, Linked references are available on JSTOR for this article: A Model of Cell Killing by Low-dose-rate Radiation Including Repair of Sublethal Damage, *G2 Block*, and, 124 (1990), pp. 201–207.
- [79] Y. Matsuya, S.J. McMahon, K. Tsutsumi, K. Sasaki, G. Okuyama, Y. Yoshii, R. Mori, J. Oikawa, K.M. Prise, H. Date, Investigation of dose-rate effects and cell-cycle distribution under protracted exposure to ionizing radiation for various dose-rates, *Sci. Rep.* 8 (2018) 8287, <https://doi.org/10.1038/s41598-018-26556-5>.
- [80] K. Cheng, M. Sano, C.H. Jenkins, G. Zhang, D. Vernekohl, W. Zhao, C. Wei, Y. Zhang, Z. Zhang, Y. Liu, Z. Cheng, L. Xing, Synergistically enhancing the therapeutic effect of radiation therapy with radiation activatable and reactive oxygen species-releasing nanostructures, *ACS Nano* 12 (2018) 4946–4958, <https://doi.org/10.1021/acsnano.8b02038>.
- [81] Y. Dou, Y. Guo, X. Li, X. Li, S. Wang, L. Wang, G. Lv, X. Zhang, H. Wang, X. Gong, J. Chang, Size-tuning ionization to optimize gold nanoparticles for simultaneous enhanced CT imaging and radiotherapy, *ACS Nano* 10 (2016) 2536–2548, <https://doi.org/10.1021/acsnano.5b07473>.
- [82] M.E. Werner, J.A. Copp, S. Karve, N.D. Cummings, R. Sukumar, C. Li, M.E. Napier, R.C. Chen, A.D. Cox, A.Z. Wang, Folate-targeted polymeric nanoparticle formulation of docetaxel is an effective molecularly targeted radiosensitizer with efficacy dependent on the timing of radiotherapy, *ACS Nano* 5 (2011) 8990–8998, <https://doi.org/10.1021/nn203165z>.
- [83] L. Chan, P. Gao, W. Zhou, C. Mei, Y. Huang, X.F. Yu, P.K. Chu, T. Chen, Sequentially triggered delivery system of black phosphorus quantum dots with surface charge-switching ability for precise tumor Radiosensitization, *ACS Nano* (2018), <https://doi.org/10.1021/acsnano.8b06483>.
- [84] H. Chaachouay, P. Ohneseit, M. Toulany, R. Kehlbach, G. Multhoff, H.P. Rodemann, Autophagy contributes to resistance of tumor cells to ionizing radiation, *Radiother. Oncol.* 99 (2011) 287–292, <https://doi.org/10.1016/j.radonc.2011.06.002>.
- [85] O. Zabinnyk, M. Yezhelyev, O. Seleverstov, Nanoparticles as a novel class of autophagy activators, *Autophagy* 3 (2007) 278–281, <https://doi.org/10.4161/auto.3916>.
- [86] A. Meidanchi, O. Akhavan, S. Khoei, A.A. Shokri, Z. Hajikarimi, N. Khansari, ZnFe₂O₄ nanoparticles as radiosensitizers in radiotherapy of human prostate cancer cells, *Mater. Sci. Eng. C* 46 (2015) 394–399, <https://doi.org/10.1016/j.msec.2014.10.062>.